

Article

# Effect of La<sup>3+</sup> Modification on the Electrochemical Performance of Na<sub>3</sub>V<sub>2</sub>(PO<sub>4</sub>)<sub>2</sub>F<sub>3</sub>

Nina V. Kosova <sup>1,\*</sup> , Daria O. Rezepova <sup>1</sup> and Nicolas Montroussier <sup>2</sup>

<sup>1</sup> Institute of Solid State Chemistry and Mechanochemistry SB RAS, 18 Kutateladze, 630128 Novosibirsk, Russia; rezepova\_do@yahoo.com

<sup>2</sup> Ecole Nationale Supérieure de Chimie de Lille, CS 90108, 59652 Villeneuve d'Ascq CEDEX, France; nicolasmontroussier@gmail.com

\* Correspondence: n.v.kosova@ya.ru or kosova@solid.nsc.ru; Tel.: +7-383-233-2410 (ext. 1115)

Received: 25 May 2018; Accepted: 29 June 2018; Published: 9 July 2018



**Abstract:** La<sup>3+</sup> modification of Na<sub>3</sub>V<sub>2</sub>(PO<sub>4</sub>)<sub>2</sub>F<sub>3</sub> was performed by the direct mechanochemically assisted solid-state synthesis of the Na<sub>3</sub>V<sub>2-x</sub>La<sub>x</sub>(PO<sub>4</sub>)<sub>2</sub>F<sub>3</sub> compositions, and by the LaPO<sub>4</sub> coating of the as-prepared Na<sub>3</sub>V<sub>2</sub>(PO<sub>4</sub>)<sub>2</sub>F<sub>3</sub> via the precipitation method. It has been shown that no noticeable substitution of the V<sup>3+</sup> ions by the La<sup>3+</sup> ions occurs in the Na<sub>3</sub>V<sub>2</sub>(PO<sub>4</sub>)<sub>2</sub>F<sub>3</sub> structure under the synthesis conditions; meanwhile, the introduction of the La<sup>3+</sup> ions into the reagent mixture leads to the formation of the LaPO<sub>4</sub> phase, and accordingly, an increase in the NaF/VPO<sub>4</sub> ratio. The latter results in the formation of the Na<sub>3</sub>PO<sub>4</sub> and Na<sub>3</sub>VF<sub>6</sub> surface impurity phases, which possess high ionic and electronic conductivity, respectively, and significantly enhances the electrical conductivity and the cycling performance of the composite cathode material both in Na and Li cells, while simple surface modification of Na<sub>3</sub>V<sub>2</sub>(PO<sub>4</sub>)<sub>2</sub>F<sub>3</sub> by LaPO<sub>4</sub> via precipitation does not.

**Keywords:** Na<sub>3</sub>V<sub>2</sub>(PO<sub>4</sub>)<sub>2</sub>F<sub>3</sub>; mechanical activation; La<sup>3+</sup> modification; cycling in Na<sup>+</sup> and Li<sup>+</sup> cells

## 1. Introduction

Among polyanionic compounds suitable for utilization as the cathode materials in the Na-ion batteries, the mixed-valence sodium vanadium fluorophosphates with a general formula of Na<sub>3</sub>V<sub>2</sub><sup>3+x</sup>O<sub>2x</sub>(PO<sub>4</sub>)<sub>2</sub>F<sub>3-2x</sub> (0 ≤ x ≤ 1) [1] are the most attractive, due to their high average operating voltage 3.8–3.9 V vs. Na<sup>+</sup>/Na, high theoretical capacity of 128 mAh·g<sup>-1</sup>, and exceptional electrochemical stability upon cycling. Na<sub>3</sub>V<sub>2</sub>(PO<sub>4</sub>)<sub>2</sub>F<sub>3</sub> is the end member of this series with x = 0; it has the highest average operating voltage of 3.89 V vs. Na<sup>+</sup>/Na [2]. Theoretical energy density of Na<sub>3</sub>V<sub>2</sub>(PO<sub>4</sub>)<sub>2</sub>F<sub>3</sub> is 507 Wh/kg, which is comparable with that of LiFePO<sub>4</sub> (580 Wh·kg<sup>-1</sup>) and LiMn<sub>2</sub>O<sub>4</sub> (480 Wh·kg<sup>-1</sup>). However, the polyanionic cathode materials usually exhibit lower electrical conductivity than the corresponding oxides, that worsens their high-rate capability. Indeed, the electrical conductivity of Na<sub>3</sub>V<sub>2</sub>(PO<sub>4</sub>)<sub>2</sub>F<sub>3</sub> is only σ = 1.2·10<sup>-7</sup> S·cm<sup>-1</sup> with the electronic conductivity being much lower than the ionic one (2·10<sup>-11</sup> S·cm<sup>-1</sup> vs. 1.2·10<sup>-7</sup> S·cm<sup>-1</sup>) [3]. Therefore, the enhancement of the electronic conductivity of Na<sub>3</sub>V<sub>2</sub>(PO<sub>4</sub>)<sub>2</sub>F<sub>3</sub> is of higher priority.

Several approaches are known to improve electrical conductivity, and hence, the electrochemical properties of cathode materials such as surface and bulk modification. Surface modification is usually carried out by electroconductive carbon. However, the carbon coating approach has no beneficial effects on the bulk electronic conductivity and alkali ion mobility. Meanwhile, the bulk modification realized by homo- or heterovalent doping can influence the conductivity, voltage, capacity, and the rate capability of the electrode materials due to the changes in their intrinsic characteristics, including crystal and electronic structure, and affect the size of the alkali-ion diffusion channels. Depending on the chosen atom-dopant, one can consider n-doping, which introduces occupied electronic states close

to the conduction band (CB), and p-doping, which introduces empty states close to the valence band (VB), thus changing the Fermi level, and the chemical and physical properties.

In recent years, a lot of experimental studies have been made on electrode materials for lithium-ion batteries tuned with rare earth elements (RE)—Y, La, Ce, Nd, Sm, Yb, etc., known for their large radius, high charge, and strong self-polarization ability. Among studied materials there are  $\text{Li}_3\text{V}_2(\text{PO}_4)_3$  [4],  $\text{LiCoO}_2$  [5],  $\text{LiNi}_{1/3}\text{Co}_{1/3}\text{Mn}_{1/3}\text{O}_2$  [6],  $\text{LiFePO}_4$  [7],  $\text{LiMn}_2\text{O}_4$  [8,9], etc. The introduction of the RE ions into the structure of the electrode materials leads to an increase in the unit cell volume due to the significant difference between ionic radii of d-metal (about 0.53–0.78 Å) and RE (about 0.87–1.03 Å), and the sizes of the alkali ion diffusion channels. Such changes cause a facile Li-ion diffusion, and as a result, increase electrical conductivity. In general, in order to form an extended region of substitutional solid solutions, the difference in ionic radii of atoms must not exceed 15% (the Hume-Rothery rule). However, in some cases, metal ions are able to replace one another in a limited range of compositions, although the difference in their radii exceeds 60% [10]. The influence of the  $\text{Ce}^{4+}$ - and  $\text{La}^{3+}$ -doping on the crystal and electronic structure of  $\text{LiCoO}_2$  has been investigated by the first-principles calculations [11]. The results indicated that  $\text{Ce}^{4+}$  and  $\text{La}^{3+}$ -doped  $\text{LiCoO}_2$  has expanded  $\text{Li}^+$  slab distances, thus decreasing the  $\text{Li}^+$  migration energy barrier; the diffusion coefficient was improved by 4 and 7 orders of magnitude, respectively. The calculations of the electronic structure showed that the doped samples possess a smaller band gap compared to pure  $\text{LiCoO}_2$ .

In the case of sodium-vanadium fluorophosphates, the surface modification with different carbon materials was widely studied and some promising results in the improvement of their electrochemical properties were achieved [12–14]. In contrast, there are only a few works on the effect of the coating by inorganic materials on their electrochemical properties. It has been shown that the  $\text{RuO}_2$ -coated  $\text{Na}_3\text{V}_2\text{O}_2(\text{PO}_4)_2\text{F}$  displays the charge-transfer resistance which is more than 4 times lower compared to the bare material, higher reversible capacity, and better rate capability [15]. On the other hand, the bulk modification of  $\text{Na}_3\text{V}_2(\text{PO}_4)_2\text{F}_3$  was conducted by a partial substitution of  $\text{V}^{3+}$  ( $r_{\text{V}^{3+}} = 0.64$  Å) by  $\text{Al}^{3+}$  ( $r_{\text{Al}^{3+}} = 0.54$  Å) [16,17], which stabilizes its crystal structure and increases the operating voltage [16]. Interestingly, the Al-doped  $\text{Na}_3\text{V}_{2-z}\text{Al}_z(\text{PO}_4)_2\text{F}_3$  material exhibits improved kinetics and an additional  $\text{Na}^+$  ion insertion at low voltages up to the  $\text{Na}_4\text{V}_{2-z}\text{Al}_z(\text{PO}_4)_2\text{F}_3$  composition due to the decreased energy barrier [17]. A successful doping of  $\text{Na}_3\text{V}_2(\text{PO}_4)_2\text{F}_3$  by the  $\text{Y}^{3+}$  ions ( $r_{\text{Y}^{3+}} = 0.9$  Å) leads to an enhancement of its electrical conductivity and electrochemical properties [18]. The excellent rate performance of  $\text{Na}_3\text{V}_{1.9}\text{Y}_{0.1}(\text{PO}_4)_2\text{F}_3/\text{C}$  could be a consequence of two factors: the enlarged diffusion channels for the  $\text{Na}^+$  ions due to the expanded NVPF lattice parameters by the larger  $\text{Y}^{3+}$  ions, and the improvement of the intrinsic electronic conductivity due to the weaker Y–O bond compared to the V–O bond [18].

In both cases, surface modification with  $\text{RuO}_2$  and ion doping with RE ( $\text{Y}^{3+}$ ), the mechanism of the improvement of the  $\text{Na}_3\text{V}_2(\text{PO}_4)_2\text{F}_3$  behavior is not well understood yet. Study of doping and coating strategies is of great significance for the further improvement of the electrochemical performance of  $\text{Na}_3\text{V}_2(\text{PO}_4)_2\text{F}_3$ . Based on these considerations, in the present work, we studied the effect of the  $\text{La}^{3+}$  modification on the conductive and electrochemical properties of the  $\text{Na}_3\text{V}_2(\text{PO}_4)_2\text{F}_3$  cathode material.

## 2. Results and Discussion

Figure 1 shows the XRD patterns of the initial  $\text{Na}_3\text{V}_2(\text{PO}_4)_2\text{F}_3$  (further referred as NVPF) and the La-modified products  $\text{Na}_3\text{V}_{2-x}\text{La}_x(\text{PO}_4)_2\text{F}_3$  with  $x = 0.02, 0.05$  (hereinafter, NVPF-La02 and NVPF-La05, respectively) prepared by the mechanochemically assisted solid-state synthesis (see Section 3). All the samples are well-crystallized; however, only NVPF is a single-phase material ascribed to  $\text{Na}_3\text{V}_2(\text{PO}_4)_2\text{F}_3$ . On the X-ray patterns of the other two samples, the reflections of  $\text{LaPO}_4$  [PDF 00-035-0731],  $\text{Na}_3\text{VF}_6$  [PDF 00-029-1286], and  $\text{Na}_3\text{PO}_4$  (including the cubic  $\gamma\text{-Na}_3\text{PO}_4$  [PDF 01-031-1323] and the tetragonal  $\text{Na}_3\text{PO}_4$  [PDF 01-072-7303] modifications) are present. The inset in Figure 1 clearly demonstrates that the position of the reflections of the main  $\text{Na}_3\text{V}_2(\text{PO}_4)_2\text{F}_3$  phase

do not change for the La-modified samples, evidencing that doping has not been realized because of a large difference in the ionic radii of  $\text{La}^{3+}$  (1.03 Å) and  $\text{V}^{3+}$  (0.64 Å).

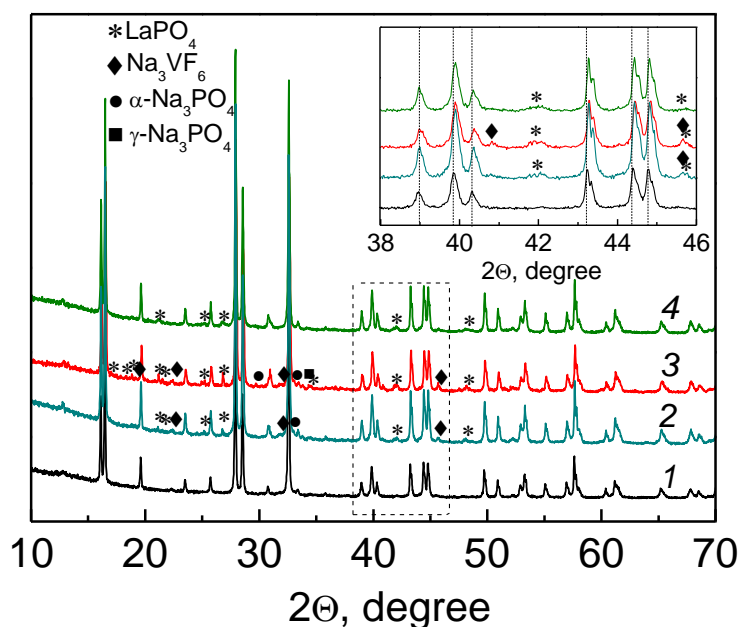


**Figure 1.** XRD patterns of the pristine NVPF (1) and the products obtained upon  $\text{La}^{3+}$  modification: NVPF-La02 (2), NVPF-La05 (3), NVPF/LPO (4).

The structure of  $\text{Na}_3\text{V}_2(\text{PO}_4)_2\text{F}_3$  is composed of the  $\text{VO}_4\text{F}_2$  octahedra, which are bridged together by one F atom forming the  $\text{V}_2\text{O}_8\text{F}_3$  bioctahedra, alternately connected by the  $\text{PO}_4$  tetrahedra. This results in a stable 3D framework, in which the  $\text{Na}^+$  ions can migrate along the [110] and [1-10] directions. The structure can be described using two space groups: the tetragonal  $P4_2/mnm$  and the orthorhombic  $Amam$  ones. The latter was proposed by Bianchini et al. [19] using synchrotron radiation; it is the most accurate to consider a small orthorhombic distortion in  $\text{Na}_3\text{V}_2(\text{PO}_4)_2\text{F}_3$  ( $b/a = 1.002$ ). This structure preserves the framework but modifies the distribution of the  $\text{Na}^+$  ions between three crystallographic positions in contrast to the  $P4_2/mnm$  S.G. with two sodium positions. Figure 2 displays the Rietveld refined XRD pattern of NVPF-La05 with the quantitative phase analysis using the  $P4_2/mnm$  S.G., which is commonly used to describe the structure of  $\text{Na}_3\text{V}_2(\text{PO}_4)_2\text{F}_3$  using the data of the regular XRD. The refined lattice parameters of the  $\text{Na}_3\text{V}_2(\text{PO}_4)_2\text{F}_3$  main phase in all the samples along with the mass content of the impurities are shown in Table 1. As can be seen, the lattice parameters of  $\text{Na}_3\text{V}_2(\text{PO}_4)_2\text{F}_3$  in NVPF-La02 and NVPF-La05 coincide with that for pristine NVPF and are close to the literature data [20]. Moreover, the estimated mass content of the  $\text{LaPO}_4$  impurity is very close to the experimental amounts of  $\text{LaPO}_4$  (1.1 wt % (2.1 mol %) and 2.7 wt % (5 mol %)) introduced into the NVPF-La02 and NVPF-La05 reagent mixtures, respectively. A slight deviation from the expected values comes from the presence of the other impurities:  $\text{Na}_3\text{VF}_6$  and  $\text{Na}_3\text{PO}_4$ , which were not included in the refinement process in the case of NVPF-La02, because of their negligible quantities. Based on the observed results, we can conclude that the crystalline  $\text{LaPO}_4$  and sodium-containing impurities are formed in the NVPF-La0.02 and NVPF-La0.05 samples, instead of the expected substitution  $\text{V}^{3+}$  for  $\text{La}^{3+}$ .

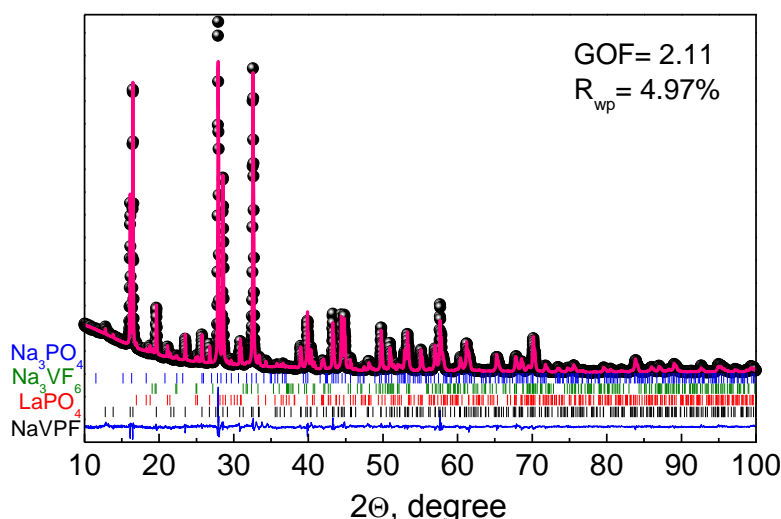


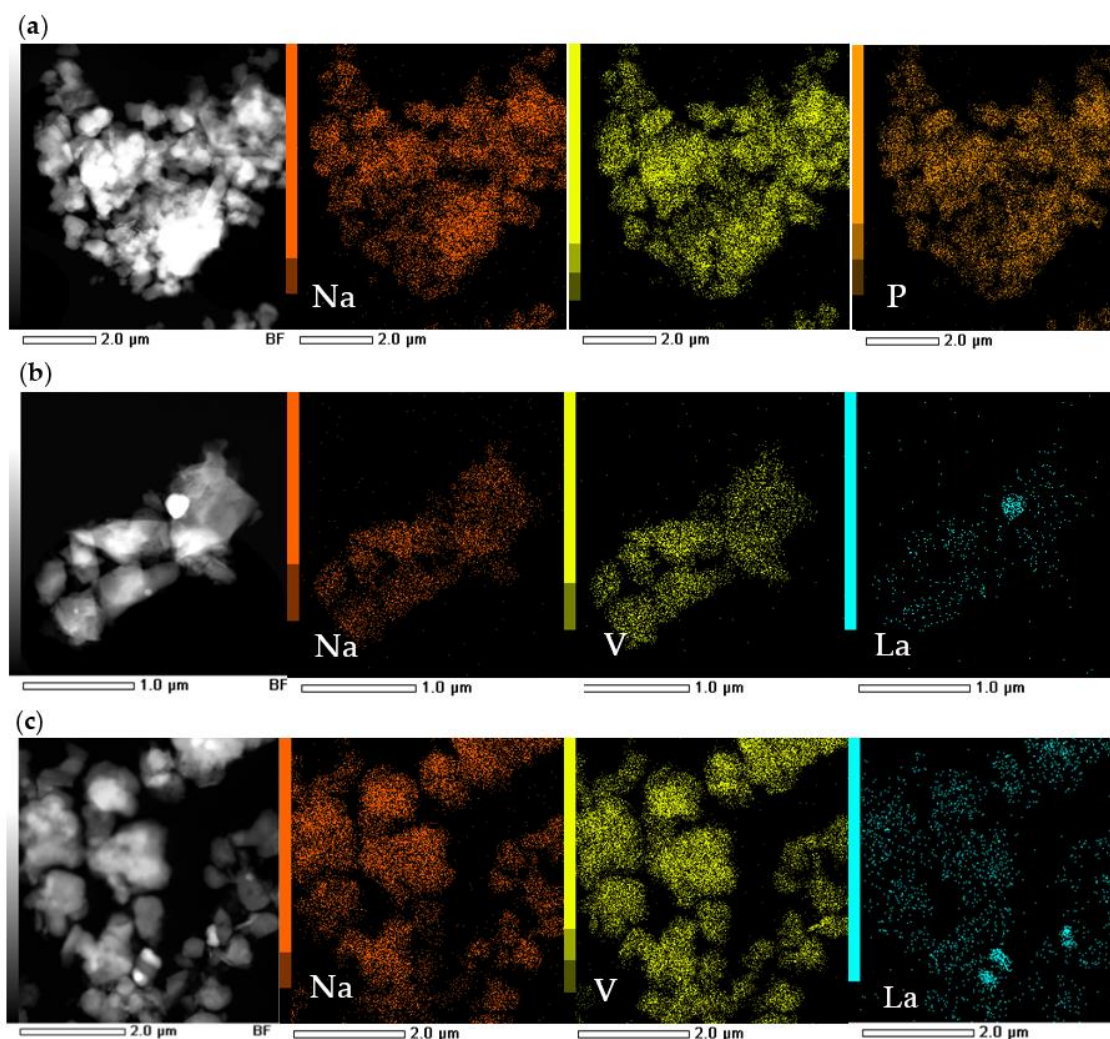
Figure 2. Rietveld refined XRD pattern of the NVPF-La05 sample.

Table 1. Phase composition of the as-prepared samples and the Rietveld refined XRD lattice parameters of the  $\text{Na}_3\text{V}_2(\text{PO}_4)_2\text{F}_3$  main phase.

	NVPF	NVPF-La02	NVPF-La05	NVPF/LPO
$\text{Na}_3\text{V}_2(\text{PO}_4)_2\text{F}_3$ , wt %	100	99.09(5)	93.41(25)	97.55(7)
$\text{Na}_3\text{VF}_6$ , wt %	-	-	2.20(15)	-
$\text{Na}_3\text{PO}_4$ (total), wt %	-	-	2.01(19)	-
$\text{LaPO}_4$ , wt %	-	0.91(5)	2.38(4)	2.45(7)
$a$ , Å	9.0393(1)	9.0401(1)	9.03702(9)	9.0390(1)
$c$ , Å	10.7520(2)	10.7494(2)	10.7494(2)	10.7512(2)
$V$ , Å <sup>3</sup>	878.54(2)	878.48(1)	877.88(2)	878.42(3)

The  $\text{LaPO}_4$  surface coating of NVPF was performed according to the procedure described in Refs. [21,22] with minor changes (see Materials and Methods). Based on the XRD results (Figure 1) and the quantitative phase analysis of the coated sample (hereinafter referred as NVPF/LPO) using the Rietveld method (Table 1), it was found that the as-obtained composite material contains only two phases:  $\text{Na}_3\text{V}_2(\text{PO}_4)_2\text{F}_3$  and  $\text{LaPO}_4$ . The reflection positions of the main phase maintain unchanged (see the insert in Figure 1), and the estimated mass amount of  $\text{LaPO}_4$  corresponds to the theoretical value (2.5 wt % (4.5 mol %)) (Table 1).

The spatial distribution of the elements in the NVPF-La05 and NVPF/LPO samples was studied by STEM combined with the EDX element mapping. As follows from Figure 3, the sodium and vanadium are uniformly distributed in all the samples.  $\text{LaPO}_4$  forms the individual crystallites with an average particle size of 200–300 nm, which are randomly distributed on the surface of the particles of the NVPF-La05 sample. For the coated sample, the  $\text{LaPO}_4$  surface distribution is also not uniform.



**Figure 3.** STEM/EDS element mapping images of NVPF (a); NVPF-La05 (b); and NVPF/LPO (c).

Figures 4a,c show the initial charge and discharge profiles, and Figure 4b,d display the high-rate performance of pristine NVPF and the  $\text{LaPO}_4$ -modified samples prepared by direct solid-state synthesis (NVPF-La05) and by the coating procedure (NVPF/LPO) in Na and Li cells. The charge-discharge profiles of all the samples in the 3.0–4.5 V range exhibit a rather similar shape. The curves consist of two pseudo-plateaus at the average voltages of 3.6–3.7 V and 4.2 V for a Na cell, and at a voltage  $\sim 0.2$  V higher for a Li cell. This similarity evidences that NVPF is a single electrochemically active phase within this voltage range. It is seen that polarization is rather small for all three samples, indicating facile alkali-ion (de)insertion reactions. The discharge capacity of the NVPF, NVPF-La05, and NVPF/LPO samples at the C/10 rate are equal to  $111 \text{ mAh}\cdot\text{g}^{-1}$ ,  $100 \text{ mAh}\cdot\text{g}^{-1}$ ,  $108 \text{ mAh}\cdot\text{g}^{-1}$  in a Na cell and to  $118 \text{ mAh}\cdot\text{g}^{-1}$ ,  $107 \text{ mAh}\cdot\text{g}^{-1}$ ,  $117 \text{ mAh}\cdot\text{g}^{-1}$  in a Li cell, respectively. Although the initial discharge capacity of NVPF-La05 is smaller than that of the pristine sample, this value corresponds to the mass quantity of the electrochemically active component— $\text{Na}_3\text{V}_2(\text{PO}_4)_2\text{F}_3$ —in this sample. Vice versa, this sample is characterized by the best high-rate performance. When the cycling rate is increased to 1C, the specific discharge capacity of NVPF-La05 is  $92 \text{ mAh}\cdot\text{g}^{-1}$  when cycled in a Na-cell, and  $103 \text{ mAh}\cdot\text{g}^{-1}$  when cycled in a Li-cell. At the 5C rate, the material shows the capacity of  $41 \text{ mAh}\cdot\text{g}^{-1}$  and  $77 \text{ mAh}\cdot\text{g}^{-1}$  when cycled in Na and Li cells, respectively. For comparison, the specific discharge capacity of the pristine sample NVPF is  $85 \text{ mAh}\cdot\text{g}^{-1}$  in a Na cell and  $106 \text{ mAh}\cdot\text{g}^{-1}$  in a Li cell at 1C;  $21 \text{ mAh}\cdot\text{g}^{-1}$  and  $32 \text{ mAh}\cdot\text{g}^{-1}$  in Na and Li cells at 5C. The behavior of the  $\text{LaPO}_4$ -coated

sample is close to that of the pristine material: the specific discharge capacity is  $16 \text{ mAh}\cdot\text{g}^{-1}$  and  $51 \text{ mAh}\cdot\text{g}^{-1}$  at the 5C rate when cycled in Na and Li cells, respectively.

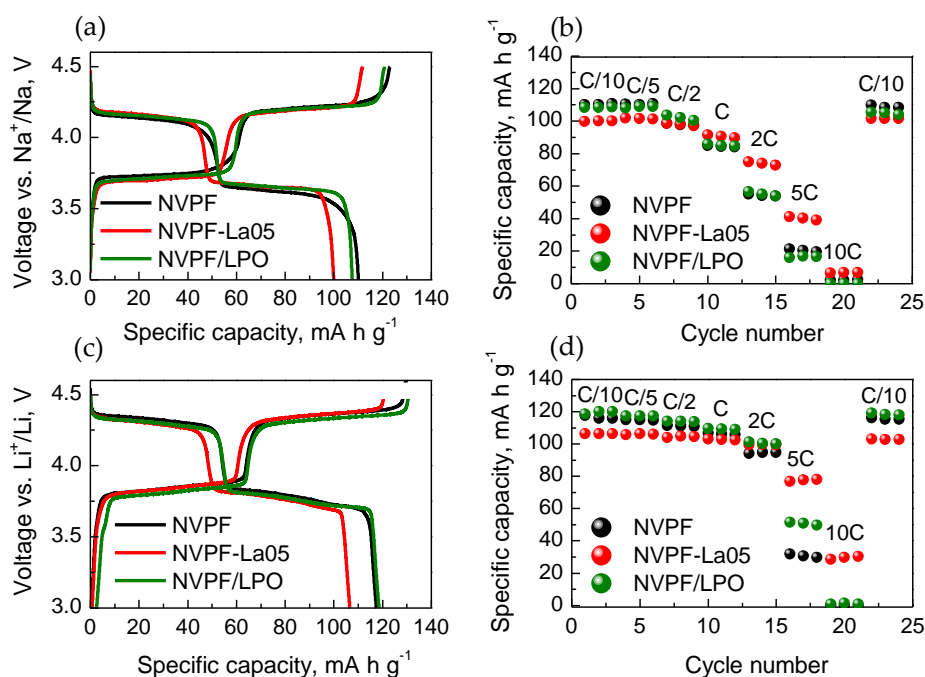


**Figure 4.** Second charge-discharge profiles at the C/10 rate (a,c) and discharge capacity vs. cycling rate (C/10–10C) plots (b,d) of NVPF, NVPF-La05 and NVPF/LPO upon cycling within the 3.0–4.5 V range in Na (a,b) and Li (c,d) cells.

The improved cyclability of NVPF-La05 at high rates is associated with an increase in its electrical conductivity. There are some publications devoted to the use of  $\text{LaPO}_4$  as a coating material to increase the high-rate capability of the lithium-rich cathode materials. However, the improvement was related to the protective activity of  $\text{LaPO}_4$  from the electrode-electrolyte interaction [21,22]. On the other hand, some authors associate it with the increase in electrical conductivity due to the high ionic conductivity of  $\text{LaPO}_4$  [23], but this statement is contradictory [24]. We were unable to find information on the high ionic conductivity of  $\text{LaPO}_4$ . Moreover, the precipitation of  $\text{LaPO}_4$  on the surface of the pristine NVPF material does not result in an improvement of its cyclability at high rates (Figure 4b,d).

Interestingly, the effect is more pronounced upon cycling the materials in a Li cell, when the  $\text{Li}^+/\text{Na}^+$  mixed electrolyte is formed after the first charge. This phenomenon may indicate a better kinetic of the mixed intercalation of the  $\text{Li}^+$  and  $\text{Na}^+$  ions. The authors [25] have shown that for the alkali ions of different size the variation in the reaction energetics for insertion/extraction in  $\text{AVPO}_4\text{F}$  may arise from the different contributions of the ion desolvation on the one hand, and transition of ions through the adsorbate layer/electrode interface on the other. Since the ionic radius of the  $\text{Li}^+$  ions is smaller than that of the  $\text{Na}^+$  ions, they have higher desolvation energy, but at the same time, they can more easily penetrate through the SEI. Earlier, we showed that  $\text{Na}_3\text{V}_2(\text{PO}_4)_2\text{F}_3$  displayed good cycleability and high-rate capability when cycled in a hybrid Na/Li cell [26]. The study of the structure and the composition of the charged and discharged samples pointed to the preservation of the initial structure, the occurrence of a negligible Na/Li electrochemical exchange, and a predominant sodium-based cathode reaction. Thus, a better kinetics of the cooperative Na/Li (de)intercalation in the mixed electrolyte might be explained by a competitive effect of the desolvation energy and a penetration rate through the SEI.

In order to find the reason of the high-rate capability improvement of NVPF-La05, EIS measurements were performed. Figure 5 represents the Nyquist plots of the pristine NVPF,

the La-modified NVPF-La05 and coated NVPF/LPO samples, and the inset in Figure 5 shows the high-frequency region. The impedance spectra consist of two semicircles; the corresponding equivalent circuit scheme is presented in Figure 5. The first part ( $R_1C_1$ ) corresponds to the bulk resistance and the capacity of the individual grains (crystallites) of the polycrystalline samples, and the second part ( $R_2C_2$ ) to the resistance and capacity of the grain boundaries. NVPF-La05 possesses the lowest total resistance, which is about two orders of magnitude lower than those of the pristine NVPF and NVPF/LPO samples. This correlates with the nice high-rate cycling performance of NVPF-La05, and the worse performance of NVPF/LPO, thereby confirming the low electrical conductivity of  $\text{LaPO}_4$ .

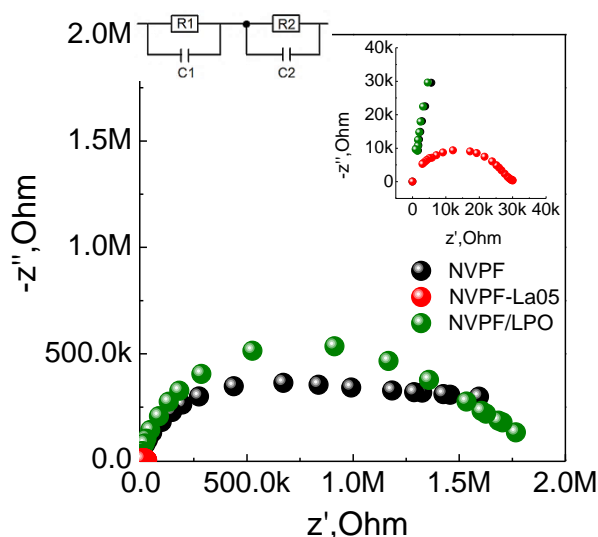


**Figure 5.** Electrochemical impedance spectra of NVPF, NVPF-La05 and NVPF/LPO.

It has been shown that, besides the formation of the surface  $\text{LaPO}_4$  phase, NVPF-La05 has additional impurity phases containing sodium, vanadium and phosphorous ions, while NVPF/LPO does not. Since the substitution of  $\text{V}^{3+}$  by  $\text{La}^{3+}$  in the  $\text{Na}_3\text{V}_2(\text{PO}_4)_2\text{F}_3$  structure does not occur, the  $\text{NaF}/\text{VPO}_4$  ratio in NVPF-La05 becomes slightly higher than in the stoichiometric one ( $>3/2$ ). We assumed that such non-stoichiometry could lead to the formation of surface Na-V-P impurity phases, probably with high conductivity, which influences the electrical conductivity of the cathode material, rather than that of  $\text{LaPO}_4$ .

To confirm this assumption, we prepared another sample with a highly stoichiometric composition  $\text{Na}_{1.75}\text{V}(\text{PO}_4)\text{F}_{1.75}$  ( $\text{N}_{1.75}\text{VPF}_{1.75}$ ) corresponding to  $\text{Na}_{3.5}\text{V}_2(\text{PO}_4)_2\text{F}_{3.5}$  with the  $\text{NaF}/\text{VPO}_4$  ratio close to that in NVPF-La05, using the same synthesis procedure. Figure 6 represents the results of XRD, EIS, and the discharge capacity vs. cycling rate ( $C/10$ – $10C$ ) plots for  $\text{N}_{1.75}\text{VPF}_{1.75}$  cycled in the Na and Li cells in comparison with the pristine NVPF and NVPF-La05. According to the XRD data, the sample contains the same impurity phases as those observed in NVPF-La05, except  $\text{LaPO}_4$ :  $\text{Na}_3\text{VF}_6$ —7.1(3)% and  $\text{Na}_3\text{PO}_4$ —12.2(7)%. The Rietveld refined lattice parameters of the main phase— $\text{Na}_3\text{V}_2(\text{PO}_4)_2\text{F}_3$  (80.7(6)%) are as follows:  $a = 9.0389(2)$  Å,  $b = 10.7533(3)$  Å,  $V = 878.55(4)$  Å<sup>3</sup>, which match well with those of the pristine NVPF sample. In Figure 6b, the Nyquist plots of the NVPF-La05 and  $\text{N}_{1.75}\text{VPF}_{1.75}$  samples are compared in the high-frequency region. Both spectra have similar semicircles. The capacitance calculated from the maximum frequency ( $\omega = 1/\text{RC}$ ) is about  $4 \cdot 10^{-10}$  F for both NVPF-La05 and  $\text{N}_{1.75}\text{VPF}_{1.75}$ , which is within the typical values for the grain boundaries capacitance [27]. Thus, this determines that the grain boundary resistance dominates the overall impedance. It can be seen that the total resistance for both samples is of the same order of magnitude ( $2.3 \cdot 10^4$  Ω for  $\text{N}_{1.75}\text{VPF}_{1.75}$  and  $2.9 \cdot 10^4$  Ω for NVPF-La05), which is much lower than those of the pristine (NVPF) and the  $\text{LaPO}_4$ -coated (NVPF/LPO) samples. The higher conductivity of  $\text{N}_{1.75}\text{VPF}_{1.75}$  results in its superior high-rate performance, as well as for NVPF-La05. When the cycling

rate is increased from C/10 to C, the specific discharge capacity of  $N_{1.75}VPF_{1.75}$  decreases by 7% only; this is comparable with the results obtained for NVPF-La05.

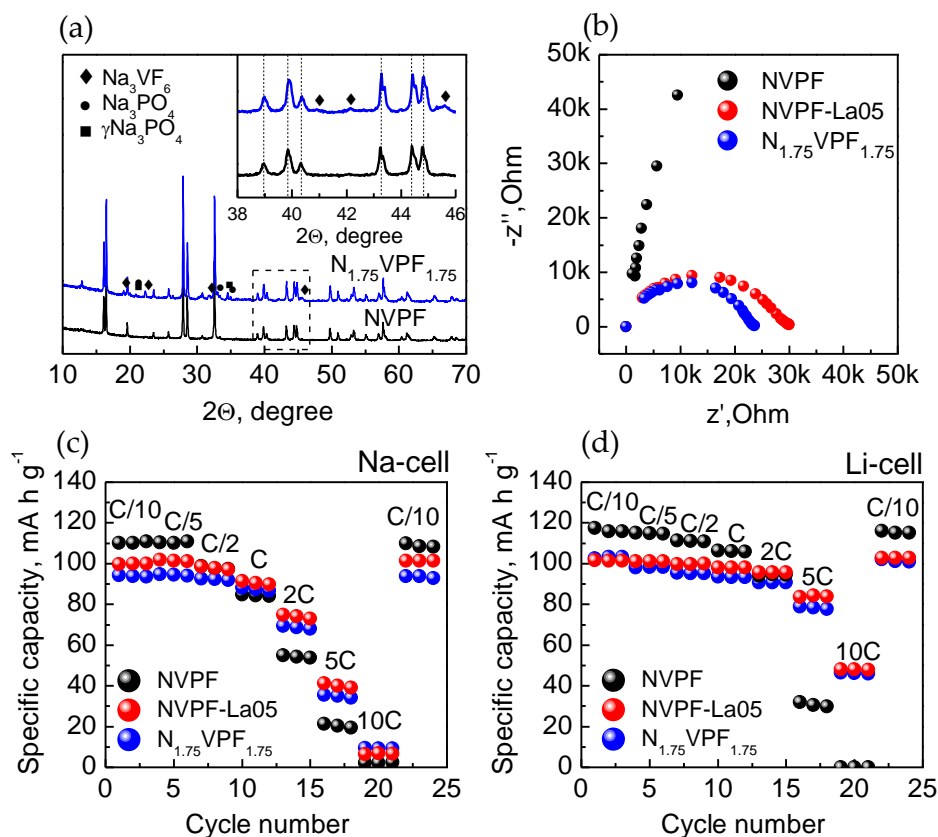


**Figure 6.** XRD pattern of  $N_{1.75}VPF_{1.75}$  (a), impedance spectra (b), and discharge capacity vs. cycling rate (C/10–10C) plots upon cycling of  $N_{1.75}VPF_{1.75}$  in the Na cell (c) and Li cell (d) within the 3.0–4.5 V range in comparison with NVPF and NVPF-La05 (d).

Summarizing all the above, our assumption regarding the positive effect of the conductive surface impurity phases on the electrochemical performance of the  $Na_3V_2(PO_4)_2F_3$  cathode material has been proven. A similar effect has been previously observed in the studies of the  $LiFePO_4$ -based cathode materials. Ceder et al. [28] created amorphous Fe-containing lithium phosphate coating with high  $Li^+$  mobility on the surface of the  $LiFePO_4$  particles and showed that this coating is responsible for the extremely high rate performance of  $LiFePO_4$  due to removing anisotropy of the surface properties and enhancing the delivery of the  $Li^+$  ions to the bulk of  $LiFePO_4$ . Nazar et al. [29] studied the doped  $Li_xZr_{0.01}FePO_4$  compositions and revealed that the surface metal-rich phosphide impurity phase could be responsible for the enhanced conductivity by formation of the percolating nano-network. The positive effect of the in situ formed surface impurity phase  $Li_3V_2(PO_4)_3$  with high ionic conductivity on the improvement of high-rate performance of  $LiVPO_4F$  was also established in our earlier study [30].

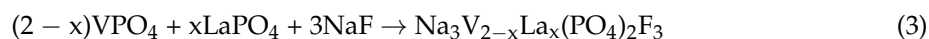
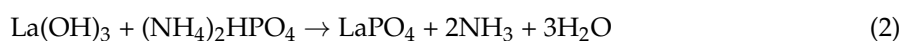
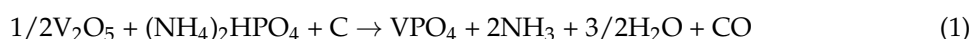
According to the literature data, the as-observed impurity phases  $Na_3PO_4$  and  $Na_3VF_6$  are characterized by high ionic and electronic conductivity, respectively [30–33].  $Na_3PO_4$  is a  $Na^+$  ion conductor with  $\sigma_{ion} \sim 10^{-7} S \cdot cm^{-1}$  at room temperature and  $\sigma_{ion} \sim 10^{-3} S \cdot cm^{-1}$  at 300 °C, having high diffusion coefficient  $D_{Na^+} \sim 1.22 \cdot 10^{-6} cm^2 \cdot s^{-1}$  [31,32], and thus, can improve the surface  $Na^+$ -ion conductivity of the  $Na_3V_2(PO_4)_2F_3$  composite cathode and facilitate the  $Na^+$ -ion exchange at the electrode-electrolyte interface. On the other hand,  $Na_3VF_6$  exhibits metal-like behavior; the resistivity of the material is  $1.1 \cdot 10^{-18} \Omega \cdot cm$  at room temperature [33]; therefore it can improve the electronic conductivity of the cathode material forming the percolating nano-network as the metal-rich

phosphides do [29]. At the same time, the formation of the amorphous sodium and lithium conductive phases cannot be excluded.

Thus, the positive effect of the surface phases on the conductivity and electrochemical performance of the  $\text{Na}_3\text{V}_2(\text{PO}_4)_2\text{F}_3$ -based cathode material has been established; however, its mechanism requires further investigation.

### 3. Materials and Methods

The  $\text{La}^{3+}$ -modification of  $\text{Na}_3\text{V}_2(\text{PO}_4)_2\text{F}_3$  (NVPF) was realized in two ways: by ‘doping’ and by surface coating. The ‘La-doped’ sodium vanadium fluorophosphates  $\text{Na}_3\text{V}_{2-x}\text{La}_x(\text{PO}_4)_2\text{F}_3$  with  $x = 0.02, 0.05$  (NVPF-La02 and NVPF-La05, respectively) were prepared by a two-step mechanochemically-assisted solid-state synthesis using  $\text{VPO}_4$  and  $\text{LaPO}_4$  as the intermediates, according to the following reactions:



The preliminary solid-state mechanical activation (MA) of the reagent mixtures was performed by means of a high-energy AGO-2 planetary mill (~900 rpm) with stainless steel jars and balls for 5 min in an Ar atmosphere. The activated mixtures (1) and (2) were annealed at 800 °C for 4 h, while the mixture (3) was heat treated at 650 °C for 2 h in an Ar flow with slow cooling to room temperature.

To prepare the  $\text{LaPO}_4$ -coated  $\text{Na}_3\text{V}_2(\text{PO}_4)_2\text{F}_3$ , the pristine sample was dispersed in distilled water under magnetic stirring for 30 min. Then stoichiometric amounts of the water solutions of  $\text{La}(\text{NO}_3)_3$  and  $(\text{NH}_4)_2\text{HPO}_4$  were consistently added to the suspension of  $\text{Na}_3\text{V}_2(\text{PO}_4)_2\text{F}_3$  under stirring for 30 min. The obtained solution was filtered, and the wet powder was dried at 90 °C in the air until the solvent was completely removed. Finally, the dried powders were further annealed at 400 °C for 4 h in the Ar atmosphere to get the  $\text{LaPO}_4$ -coated  $\text{Na}_3\text{V}_2(\text{PO}_4)_2\text{F}_3$  (hereinafter referred as NVPF/LPO). The amount of  $\text{LaPO}_4$  in the composite material was 2.5 wt %, which is close to the La content in NVPF-La05.

X-ray powder diffraction (XRD) patterns of the as-prepared samples were recorded by a D8 Advance Bruker diffractometer (Bruker AXS GmbH, Karlsruhe, Germany) with a high-rate detector Lynx Eye, Cu  $K\alpha_{1,2}$  radiation ( $\alpha_1 = 1.5406 \text{ \AA}$ ,  $\alpha_2 = 1.5445 \text{ \AA}$ ) within the 10–100° ( $2\theta$ ) range with a step of 0.02° and uptake time of 0.3–1.0 s. The structural refinement of the XRD data was carried out by the Rietveld method using the TOPAS software [34]. The procedure was started with the refinement of the lattice parameters and atomic positions of the pristine NVPF. The thermal displacement parameters for all atoms were refined just once and then fixed at their final values; the thermal parameters for the atoms of the same elements were taken to be equal. The structural refinement of the main phase in the multi-phase samples was performed in a similar manner; all thermal parameters were kept fixed at the values extracted from the structural refinement of the pristine sample. STEM-EDS mapping was carried out using a JEM-2200FS transmission electron microscope (JEOL Co., Ltd., Tokyo, Japan) with an accelerating voltage of 200 kV and magnification of 0.1 nm.

Electrochemical impedance spectroscopy (EIS) study of the as-prepared samples was performed using an LCR-meter E7-25 (MNIPI, Minsk, Belarus) in the frequency range of 25 Hz–1 MHz in pellets with the Ag electrodes at room temperature. Electrochemical cycling was performed in a galvanostatic mode both in the Na and Li cells within the 3.0–4.5 V range at the C/10–10C rates. The composite cathode materials were fabricated by mixing 75 wt % active material with 20 wt % Super P (Timcal, Bodio, Switzerland) and 5 wt % PVDF/NMP binder. The mixed slurry was then pasted onto aluminum foil, dried in a vacuum oven at 90 °C, and then cut into small circular discs to obtain working electrodes. The total amount of carbon in the cathode mass was 20 wt %; mass loading

$\sim 1.5\text{--}2.0\text{ mg}\cdot\text{cm}^{-2}$  and the electrode diameter of 10 mm were used throughout. Swagelok-type cells were assembled in an Ar-filled glove box with Na metal as an anode and 1 M NaPF<sub>6</sub> solution in a mixture of ethylene carbonate and propylene carbonate 1:1 by weight as an electrolyte for the Na cells, and with Li metal as an anode and 1 M LiPF<sub>6</sub> solution in a mixture of ethylene carbonate and dimethyl carbonate 2:1 by weight as an electrolyte for the Li cells. A glass fiber filter, Grade GF/C GE Healthcare UK Ltd., Little Chalfont, UK) was used as a separator.

#### 4. Conclusions

The Na<sub>3</sub>V<sub>2</sub>(PO<sub>4</sub>)<sub>2</sub>F<sub>3</sub> composite cathode materials modified with LaPO<sub>4</sub> were synthesized using the mechanochemically assisted solid-state synthesis and the precipitation method. It has been shown that no noticeable substitution of the V<sup>3+</sup> ions by the La<sup>3+</sup> ions occurs in the Na<sub>3</sub>V<sub>2</sub>(PO<sub>4</sub>)<sub>2</sub>F<sub>3</sub> structure under the synthesis conditions. Meanwhile, the introduction of La<sup>3+</sup> ions into the reagent mixture led to the formation of the LaPO<sub>4</sub> phase, and an increase in the NaF/VPO<sub>4</sub> ratio in the reagent mixture, which resulted in the formation of the Na<sub>3</sub>PO<sub>4</sub> and Na<sub>3</sub>VF<sub>6</sub> surface impurity phases. These phases possess high ionic and electronic conductivity, respectively, and significantly enhance the electrical conductivity and the cycling performance of the NVPF cathode material, while simple surface modification of NVPF by LaPO<sub>4</sub> via precipitation does not. Thus, the results obtained evidence that by changing the stoichiometry in the reagent mixture (a slight excess of NaF), the surface conductive impurity phases can be formed in situ, which improves the high-rate performance of the NVPF cathode material. However, the detailed mechanism of the positive effect of the surface phases on the conductivity of the Na<sub>3</sub>V<sub>2</sub>(PO<sub>4</sub>)<sub>2</sub>F<sub>3</sub>-based cathode material requires further investigation.

**Author Contributions:** N.V.K. conceived and designed the experiments; D.O.R. performed the experiments; both authors participated in the analysis of the experimental data and in writing the paper. N.M. helped to perform the synthesis experiments.

**Funding:** This research was carried out within the state Assignment to ISSCM SB RAS (project 0301-2018-0001) and was partially supported by the Russian Foundation for Basic Research and the government of the Novosibirsk region of the Russian Federation (grant No. 18-43-540022).

**Acknowledgments:** The authors are thankful to Natalia V. Bulina for registration of the XRD patterns and Arkady V. Ishchenko for the STEM EDX study.

**Conflicts of Interest:** The authors declare no conflict of interest.

#### References

1. Serras, P.; Palomares, V.; Goñi, A.; Gil de Muro, I.; Kubiak, P.; Lezama, L.; Rojo, T. High voltage cathode materials for Na-ion batteries of general formula Na<sub>3</sub>V<sub>2</sub>O<sub>2x</sub>(PO<sub>4</sub>)<sub>2</sub>F<sub>3-2x</sub>. *J. Mater. Chem.* **2012**, *22*, 22301–22308. [[CrossRef](#)]
2. Broux, T.; Bamine, T.; Fauth, F.; Simonelli, L.; Olszewski, W.; Marini, C.; Menetrier, M.; Carlier, D.; Masquelier, C.; Croguennec, L. Strong impact of the oxygen content in Na<sub>3</sub>V<sub>2</sub>(PO<sub>4</sub>)<sub>2</sub>F<sub>3-y</sub>O<sub>y</sub> (0 ≤ y ≤ 0.5) on its structural and electrochemical properties. *Chem. Mater.* **2016**, *28*, 7683–7692. [[CrossRef](#)]
3. Zhu, C.; Wu, C.; Chen, C.-C.; Kopold, P.; van Aken, P.A.; Maier, J.; Yu, Y. A high power–high energy Na<sub>3</sub>V<sub>2</sub>(PO<sub>4</sub>)<sub>2</sub>F<sub>3</sub> sodium cathode: investigation of transport parameters, rational design and realization. *Chem. Mater.* **2017**, *29*, 5207–5215. [[CrossRef](#)]
4. Zhong, S.; Liu, L.; Jiang, J.; Li, Y.; Wang, J.; Liu, J.; Li, Y. Preparation and electrochemical properties of Y-doped Li<sub>3</sub>V<sub>2</sub>(PO<sub>4</sub>)<sub>3</sub> cathode materials for lithium batteries. *J. Rare Earths* **2009**, *27*, 134–137. [[CrossRef](#)]
5. Ghosh, P.; Mahanty, S.; Basu, R.N. Lanthanum-doped LiCoO<sub>2</sub> cathode with high rate capability. *Electrochim. Acta* **2009**, *54*, 1654–1661. [[CrossRef](#)]
6. Sun, H.; Chen, Y.; Xu, C.; Zhu, D.; Huang, L. Electrochemical performance of rare-earth doped LiMn<sub>2</sub>O<sub>4</sub> spinel cathode materials for Li-ion rechargeable battery. *J. Solid State Electrochem.* **2012**, *16*, 1247–1254. [[CrossRef](#)]
7. Zhong, S.; Wang, Y.; Jiu, J.; Wan, K.; Lu, F. Synthesis and electrochemical properties of Ce-doped LiNi<sub>1/3</sub>Mn<sub>1/3</sub>Co<sub>1/3</sub>O<sub>2</sub> cathode material for Li-ion batteries. *J. Rare Earths* **2011**, *29*, 891–985. [[CrossRef](#)]

8. Wang, L.; Jiao, C.; Liang, G.; Zhao, N.; Wang, Y.; Li, L. Effect of rare earth ions doping on properties of  $\text{LiFePO}_4/\text{C}$  cathode material. *J. Rare Earths* **2014**, *32*, 895–899. [[CrossRef](#)]
9. Ram, P.; Gören, A.; Ferdov, S.; Silva, M.M.; Singhal, R.; Costa, C.M.; Sharma, R.K.; Lanceros-Méndez, S. Improved performance of rare earth doped  $\text{LiMn}_2\text{O}_4$  cathodes for lithium-ion battery applications. *New J. Chem.* **2016**, *40*, 6244–6252. [[CrossRef](#)]
10. West, A.R. *Solid State Chemistry and Its Applications*; John Wiley and Sons: New York, NY, USA, 1984.
11. Ning, F.; Xu, B.; Shi, J.; Wu, M.; Hu, Y.; Ouyang, C. Structural, electronic, and Li migration properties of RE-doped (RE = Ce, La)  $\text{LiCoO}_2$  for Li-ion batteries: A first-principles investigation. *J. Phys. Chem. C* **2016**, *120*, 18428–18434. [[CrossRef](#)]
12. Eshraghi, N.; Caes, S.; Mahmoud, A.; Cloots, R.; Vertruyen, B.; Boschini, F. Sodium vanadium (III) fluorophosphate/carbon nanotubes composite (NVPF/CNT) prepared by spray-drying: Good electrochemical performance thanks to well-dispersed CNT network within NVPF particles. *Electrochim. Acta* **2017**, *228*, 319–324. [[CrossRef](#)]
13. Liu, Q.; Meng, X.; Wei, Z.; Wang, D.; Gao, Y.; Wei, Y.; Du, F.; Chen, G. Core/double-shell structured  $\text{Na}_3\text{V}_2(\text{PO}_4)_2\text{F}_3@\text{C}$  nanocomposite as the high power and long lifespan cathode for sodium-ion batteries. *ACS Appl. Mater. Interfaces* **2016**, *8*, 31709–31715. [[CrossRef](#)] [[PubMed](#)]
14. Liu, Q.; Wang, D.; Yang, X.; Chen, N.; Wang, C.; Bie, X.; Wei, Y.; Chen, G.; Du, F. Carbon-coated  $\text{Na}_3\text{V}_2(\text{PO}_4)_2\text{F}_3$  nanoparticles embedded in a mesoporous carbon matrix as a potential cathode material for sodium-ion batteries with superior rate capability and long-term cycle life. *J. Mater. Chem. A* **2015**, *3*, 21478–21485. [[CrossRef](#)]
15. Peng, M.; Li, B.; Yan, H.; Zhang, D.; Wang, X.; Xia, D.; Guo, G. Ruthenium-oxide-coated sodium vanadium fluorophosphate nanowires as high-power cathode materials for sodium-ion batteries. *Angew. Chem. Int. Ed.* **2015**, *54*, 6452–6456. [[CrossRef](#)] [[PubMed](#)]
16. Pineda-Aguilar, N.; Gallegos-Sánchez, V.J.; Sánchez, E.M.; Torres-González, L.C.; Garza-Tovar, L.L. Aluminum doped  $\text{Na}_3\text{V}_2(\text{PO}_4)_2\text{F}_3$  via sol-gel Pechini method as a cathode material for lithium ion batteries. *J. Sol.-Gel. Sci. Technol.* **2017**, *83*, 405–412. [[CrossRef](#)]
17. Bianchini, M.; Xiao, P.; Wang, Y.; Ceder, G. Additional sodium insertion into polyanionic cathodes for higher-energy Na-ion batteries. *Adv. Energy Mater.* **2017**, *7*, 1700514. [[CrossRef](#)]
18. Liu, W.; Yi, H.; Zheng, Q.; Li, X.; Zhang, H. Y-doped  $\text{Na}_3\text{V}_2(\text{PO}_4)_2\text{F}_3$  compounds for sodium ion battery cathodes: electrochemical performance and analysis of kinetic properties. *J. Mater. Chem. A* **2017**, *5*, 10928–10935. [[CrossRef](#)]
19. Bianchini, M.; Brisset, N.; Fauth, F.; Weill, F.; Elkaim, E.; Suard, E.; Masquelier, C.; Croguennec, L.  $\text{Na}_3\text{V}_2(\text{PO}_4)_2\text{F}_3$  revisited: A high-resolution diffraction study. *Chem. Mater.* **2014**, *26*, 4238–4247. [[CrossRef](#)]
20. Gover, R.K.B.; Bryan, A.; Burns, P.; Barker, J. The electrochemical insertion properties of sodium vanadium fluorophosphate,  $\text{Na}_3\text{V}_2(\text{PO}_4)_2\text{F}_3$ . *Solid State Ion.* **2006**, *177*, 1495–1500. [[CrossRef](#)]
21. Song, H.G.; Park, Y.J.  $\text{LiLaPO}_4$ -coated  $\text{Li}[\text{Ni}_{0.5}\text{Co}_{0.2}\text{Mn}_{0.3}]\text{O}_2$  and  $\text{AlF}_3$ -coated  $\text{Li}[\text{Ni}_{0.5}\text{Co}_{0.2}\text{Mn}_{0.3}]\text{O}_2$  blend composite for lithium ion batteries. *Mater. Res. Bull.* **2012**, *47*, 2843–2846. [[CrossRef](#)]
22. Xie, Q.; Zhao, C.; Hu, Z.; Huang, Q.; Chen, C.; Liu, K.  $\text{LaPO}_4$ -coated  $\text{Li}_{1.2}\text{Mn}_{0.56}\text{Ni}_{0.16}\text{Co}_{0.08}\text{O}_2$  as a cathode material with enhanced coulombic efficiency and rate capability for lithium ion batteries. *RSC Adv.* **2015**, *5*, 77324–77331. [[CrossRef](#)]
23. Shen, C.; Zheng, J.; Zhang, B.; Han, Y.; Zhang, J.; Ming, L.; Li, H.; Yuan, X. Composite cathode material  $\beta\text{-LiVOPO}_4/\text{LaPO}_4$  with enhanced electrochemical properties for lithium ion batteries. *RSC Adv.* **2014**, *4*, 40912–40916. [[CrossRef](#)]
24. Arroyo-de Dompablo, M.E.; Amador, U.; Lozano, E.; Baetzsch, C.; Morán, E.; Fuentes, A.F. Reactivity of nano- $\text{LaPO}_4$  composites in lithium cells. *ECS Trans.* **2011**, *33*, 101–110.
25. Nikitina, V.A.; Fedotov, S.S.; Vassiliev, S.Y.; Samarin, A.S.; Khasanova, N.R.; Antipov, E.V. Transport and kinetic aspects of alkali metal ions intercalation into  $\text{AVPO}_4\text{F}$  framework. *J. Electrochem. Soc.* **2017**, *164*, A6373–A6380. [[CrossRef](#)]
26. Kosova, N.V.; Rezepova, D.O.  $\text{Na}_{1+y}\text{VPO}_4\text{F}_{1+y}$  ( $0 \leq y \leq 0.5$ ) as cathode materials for hybrid Na/Li batteries. *Inorganics* **2017**, *5*, 19–32. [[CrossRef](#)]
27. Irvine, J.T.S.; Sinclair, D.C.; West, A.R. Electroceramics: Characterization by impedance spectroscopy. *Adv. Mater.* **1990**, *2*, 132–138. [[CrossRef](#)]

28. Kang, B.; Ceder, G. Battery materials for ultrafast charging and discharging. *Nature* **2009**, *458*, 190–193. [[CrossRef](#)] [[PubMed](#)]
29. Subramanya Herle, P.; Ellis, B.; Coombs, N.; Nazar, L.F. Nano-network electronic conduction in iron and nickel olivine phosphates. *Nat. Mater.* **2004**, *3*, 147–152. [[CrossRef](#)] [[PubMed](#)]
30. Kosova, N.V.; Devyatkina, E.T.; Slobodyuk, A.B.; Gutakovskii, A.K. LiVPO<sub>4</sub>F/Li<sub>3</sub>V<sub>2</sub>(PO<sub>4</sub>)<sub>3</sub> nanostructured composite cathode materials prepared via mechanochemical way. *J. Solid State Electrochem.* **2014**, *18*, 1389–1399. [[CrossRef](#)]
31. Irvine, J.T.S.; West, A.R. Sodium ion-conducting solid electrolytes in the system Na<sub>3</sub>PO<sub>4</sub>-Na<sub>2</sub>SO<sub>4</sub>. *J. Solid State Chem.* **1987**, *69*, 126–134. [[CrossRef](#)]
32. Yin, W.-G.; Liu, J.; Duan, C.-G.; Mei, W.N.; Smith, R.W.; Hardy, J.R. Superionicity in Na<sub>3</sub>PO<sub>4</sub>: A molecular dynamics simulation. *Phys. Rev. B* **2004**, *70*. [[CrossRef](#)]
33. Reshak, A.H.; Azam, S. Density of states, optical and thermoelectric properties of perovskite vanadium fluorides Na<sub>3</sub>VF<sub>6</sub>. *J. Magn. Magn. Mater.* **2014**, *358–359*, 16–22. [[CrossRef](#)]
34. Cheary, R.W.; Coelho, A.A. A fundamental parameters approach to X-ray line-profile fitting. *J. Appl. Cryst.* **1992**, *25*, 109–121. [[CrossRef](#)]



© 2018 by the authors. Licensee MDPI, Basel, Switzerland. This article is an open access article distributed under the terms and conditions of the Creative Commons Attribution (CC BY) license (<http://creativecommons.org/licenses/by/4.0/>).